Computational Prediction of α/β Selectivities in the Pyrolysis of Oxygen-Substituted Phenethyl Phenyl Ethers

Ariana Beste,*,† A. C Buchanan III,‡ and Robert J. Harrison†,§

Computer Science and Mathematics Division, Oak Ridge National Laboratory, 1 Bethel Valley Road, Oak Ridge, Tennessee 37831-6367, Chemical Sciences Division, Oak Ridge National Laboratory, 1 Bethel Valley Road, Oak Ridge, Tennessee 37831-6197, and Department of Chemistry, University of Tennessee, Knoxville, Tennessee 37996

Received: January 25, 2008; Revised Manuscript Received: March 28, 2008

Phenethyl phenyl ether (PPE; $PhCH_2CH_2OPh$) is the simplest model for the most common β-O-4 linkage in lignin. Previously, we developed a computational scheme to calculate the α/β product selectivity in the pyrolysis of PPE by systematically exploiting error cancellation in the computation of relative rate constants. The α/β selectivity is defined as the selectivity between the competitive hydrogen abstraction reaction paths on the α- and β-carbons of PPE. We use density functional theory and employ transition state theory where we include diagonal anharmonic correction in the vibrational partition functions for low frequency modes for which a semiclassical expression is used. In this work we investigate the effect of oxygen substituents (hydroxy, methoxy) in the para position on the phenethyl ring of PPE on the α/β selectivities. The total α/β selectivity increases when substituents are introduced and is larger for the methoxy than the hydroxy substituent. The strongest effect of the substituents is observed for the α-pathway of the hydrogen abstraction by the phenoxyl chain carrying radical for which the rate increases. For the β pathway and the abstraction by the R-benzyl radical ($R = OH, OCH_3$) the rate decreases with the introduction of the substituents. These findings are compared with results from recent experimental studies.

Introduction

Lignin is a complex polymer present in all vascular plants. It cross links different plant polysaccharides giving mechanical strength to the cell wall. Large amounts of lignin are produced by the paper industry and much of it is used as a fuel. Lignin also potentially serves as a natural adsorbent[1] or as a source of syngas,[2] but alternative large scale applications have not been found yet. The isolation of lignin is difficult because of condensation and oxidation reactions occurring during the process. The nonuniqueness of the isolation process complicates the development of new economically viable applications leading to different chemical behavior of lignin depending on origin and processing techniques.[2] For reviews on the gasification and thermochemical conversion of biomass see ref 1 and references in ref 3.

Depending on the origin, lignin is naturally produced by the enzymatic polymerization of three main monolignols (*p*-coumaryl, coniferyl, and sinapyl alcohol), which are interconnected by a variety of linkages (β-O-4, β-5′, 5-5′, β-β′, etc.). The chemistry of lignin is often studied through model compounds.[3–5] The most common interunit linkage in lignin is the arylglycerol-β-aryl (β-O-4) linkage, shown in Figure 1, for which phenethyl phenyl ether (PPE) is the simplest model. Britt et al. [5] studied the pyrolysis of PPE and provided evidence for a free-radical chain mechanism to take place. The thermolysis of PPE proceeds through two competitive pathways, defined as

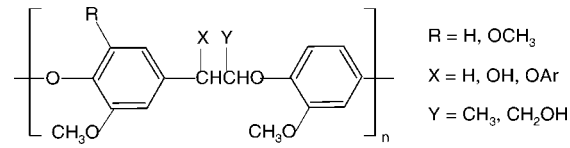

Figure 1. Arylglycerol-β-aryl ether linkage in lignin.

α/β selectivity, where hydrogen is abstracted from the α- or β-position of PPE by the chain carrying phenoxyl and benzyl radicals.

Generally, the size of even the model systems makes computational studies difficult, and we are aware of only a few computational investigations of lignin models.[6,7] In particular, the prediction of rate constants is challenging. The demand on computational resources increases with increasing system size, and the occurrence of low-frequency vibrational modes becomes more likely in larger organic molecules. With each added substructure a potential internal rotation is introduced. It has been shown that the correct treatment of low-frequency modes is crucial.[8–10] The transition states we investigate in this work have 9−11 frequencies below 100 cm^{-1}, which have large anharmonic contributions and need to be treated accordingly. Anharmonic corrections to vibrations can be calculated using perturbation theory[11] or self-consistent field methods.[12] The anharmonic frequencies and zero point energies can then be substituted for their harmonic counterparts in the expression of the harmonic quantum partition function.[13] If the internal rotation is separable from the low-frequency vibrations, the internal rotation can be described as a hindered rotor.[8,10] Because of the large number of coupled low-frequency modes in the transition states located in this work, the hindered rotor approximation is difficult to apply.

* To whom correspondence should be addressed. E-mail: bestea@ornl.gov. Phone: 865-241-3160. Fax: 865-574-0680.

† Computer Science and Mathematics Division, Oak Ridge National Laboratory.

‡ Chemical Sciences Division, Oak Ridge National Laboratory.

§ University of Tennessee.

10.1021/jp800767j CCC: $40.75
Published on Web 05/13/2008

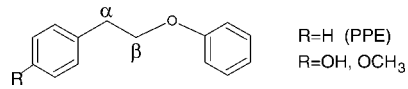

Figure 2. Oxygen-substituted phenethyl phenyl ethers (including PPE).

In previous work,[3] we developed a computational protocol to calculate α/β selectivities using transition state theory and demonstrated its reliability by calculating the overall α/β selectivity in the pyrolysis of PPE. Instead of absolute rate constants, we calculated relative rate constants, which enables us to profit from systematic error cancelation. The α- and β-pathways differ in their transition states, but the reactants are the same. The α/β selectivity is therefore determined only by activation energies and partition functions of similar transition states which makes error cancelation particularly effective. We use density functional theory (B3LYP) to accommodate the medium-size molecules. The transition states located for the pyrolysis of PPE[3] and for similar reactions[14] showed spurious imaginary frequencies that are caused by a flat potential energy surface in combination with the breakdown of the harmonic approximation. For such frequencies the harmonic partition function is not defined. Instead, we use a semiclassical partition function for which we determine the anharmonic potential by displacement along the corresponding normal mode. The diagonal anharmonic corrections are also applied for low-frequency modes, the partition functions of high-frequency modes are calculated within the harmonic quantum approximation.

While the detailed kinetic analysis of the pyrolysis of PPE as the simplest model for the β-O-4 linkage in lignin gives valuable insight,[3,5] more realistic lignin models include substituents. As shown in Figure 1, common substituents are hydroxy and methoxy groups. The effect of oxygen substituents in the pyrolysis of PPE has been studied recently by Britt et al.[15] In this work we investigate the pyrolysis of the ethers given in Figure 2. Our goal is to explain the experimentally observed substituent effects by analyzing the electronic structure of the transition states. We also want to reproduce the observed trend in the α/β selectivities and compare the influence of the substituent on the individual pathways.

Computational Details

All calculations are carried out with the NWChem program package.[16] We use the unrestricted B3LYP[17,18] functional to search for equilibrium and transition-state structures. The B3LYP functional has been successfully employed to calculate reaction barriers of similar reactions,[14] and the α/β selectivity for the hydrogen abstraction on PPE was predicted in good agreement with experiment using the B3LYP functional.[3] The grid on which the exchange-correlation contribution to the density functional is evaluated is set to be extrafine, which gives an approximate accuracy of the total energy of 10^{-8} H. A mixed basis set is used for the geometry optimizations and frequency calculations as described in ref 3 where its validity has also been shown. Single-point calculations are performed for all stationary points using the 6-311++G** basis set on all atoms. Energy differences are zero point corrected. We preoptimize the transition states with a fixed distance between the transferred hydrogen and the hydrogen donor and acceptor. We choose up to 10 starting structures per reaction distinguished by different orientations of the reactants to each other.

The computational details to calculate the α/β selectivity for the hydrogen abstraction reactions has been given previously.[3] The rate constants are calculated with transition-state theory.[19]

SCHEME 1: Chain-carrying radical reactions in the mechanism for the thermal decomposition of oxygen substituted PPE; R = H,OH,OCH$_3$

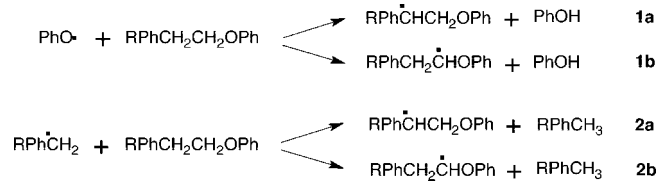

For the reactions considered in this work, we obtain multiple transition states for the same reaction, each one defining a reaction path. The rate constant is the sum over all reaction paths. Within transition-state theory, the rate constant is determined by the reaction barrier and the partition functions for translation, rotation, vibration, and electronic contribution of the reactants and transition states. We find 9−11 frequencies in the transition states to be below 100 cm^{-1} that contain significant anharmonic contributions. For frequencies that are larger than 100 cm^{-1} we use the quantum harmonic partition function; this choice has been rationalized previously.[3] For frequencies below 100 cm^{-1}, a semiclassical expression, i.e., a Wigner−Kirkwood expansion,[20] for the vibrational partition function is employed. The validity of the semiclassical expression in the experimental temperature range was tested earlier.[3] The anharmonic potential, which is incorporated in the partition function, is obtained by displacing along the normal mode. This approach allows for diagonal anharmonic corrections in the rate constants, i.e., the coupling between the modes is included on the level of the harmonic approximation. For frequencies below 20 cm^{-1}, a fourth-order polynomial fit to the potential is generated. For frequencies between 20 and 100 cm^{-1}, we compute an approximate anharmonic fourth-order potential using the energies of two geometries along the normal mode and assuming the harmonic second order force constant to be correct through first order.

Results and Discussion

We investigate the pyrolysis of hydroxy and methoxy substituted PPE, shown in Figure 2. The effect of oxygen substituents in the pyrolysis of PPE has been studied experimentally by Britt et al.[15] The initial step of the radical chain mechanism is the homolytic cleavage of the weakest bond, the aliphatic carbon oxygen bond, producing the phenoxyl radical which is one of the chain carrying radicals. The hydrogen atom is competitively abstracted from the α- or β-position of the substituted PPE by the phenoxyl radical forming the corresponding α- and β-radical, shown in reaction 1 of Scheme 1. The α-radical undergoes rapid β-scission yielding the phenoxyl radical. The β-radical is converted by 1,2 phenyl migration. The migration product reacts further to form the second chain carrying radical: the substituted benzyl radical which again abstracts hydrogen from the α- or β-position of the substituted PPE, reaction 2 of scheme 1. The overall α/β selectivity is a composite of the α/β selectivity of the hydrogen abstraction by the phenoxyl radical (reaction 1) and by the substituted benzyl radical (reaction 2). We consider 8 reactions: 1a, 1b, 2a, 2b for the hydroxy and the methoxy substituent.

A. Electronic Structure. The transition states located for the pyrolysis of R-PPE (R = OH, OCH_3) are similar to the transition states found for the pyrolysis of PPE.[3] We obtain multiple transition states for each reaction. PPE has two equivalent α-hydrogen atoms, and two equivalent β-hydrogen

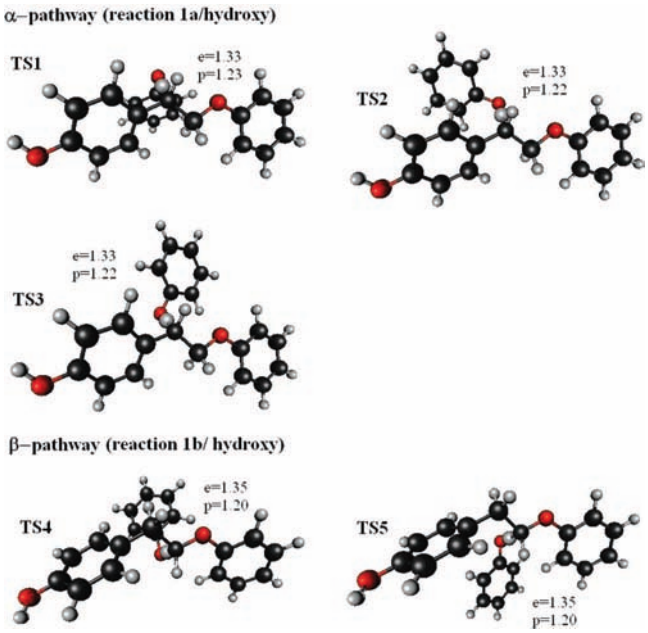

Figure 3. Transition-state geometries for hydrogen abstraction by phenoxyl radical (reaction 1) on hydroxy PPE: (α) H-PPEOH bond lengths in Å; (*β*) H-phenoxyl bond lengths in Å.

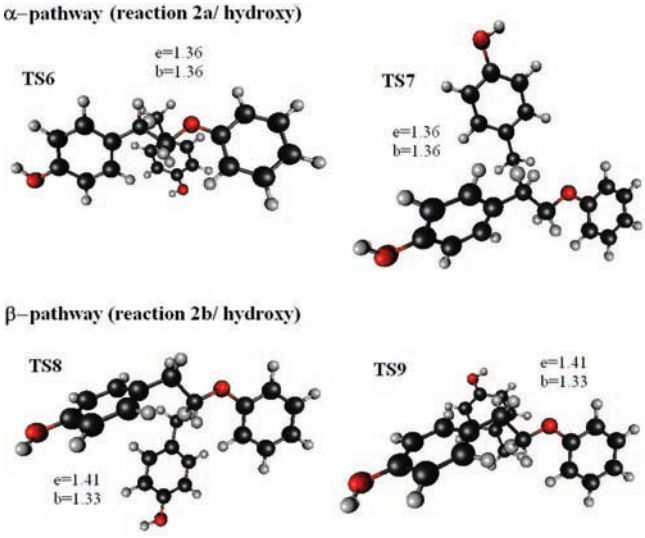

Figure 4. Transition-state geometries for hydrogen abstraction by *p*-hydroxy-benzyl radical (reaction 2) on hydroxy PPE: (α) H-PPEOH bond lengths in Å; (*β*) H-*p*-hydroxy-benzyl bond lengths in Å.

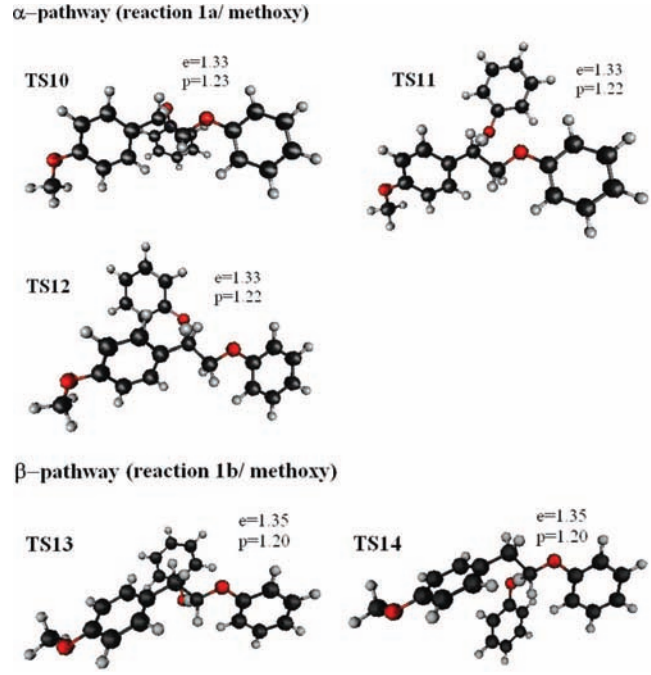

Figure 5. Transition-state geometries for hydrogen abstraction by phenoxyl radical (reaction 1) on methoxy PPE: (α) H-PPEMeO bond lengths in Å; (*β*) H-phenoxyl bond lengths in Å.

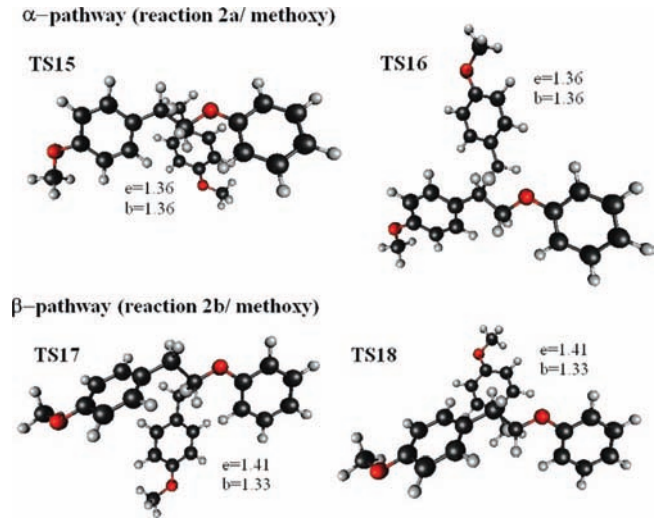

Figure 6. Transition-state geometries for hydrogen abstraction by *p*-methoxy-benzyl radical (reaction 2) on methoxy PPE; (α) H-PPEMeO bond lengths in Å; (*β*) H-*p*-methoxy-benzyl bond lengths in Å.

atoms and the radicals (phenoxyl and benzyl) can abstract from two equivalent sides. In substituted PPE the hydrogen atoms are not equivalent, and neither are the two sides of the benzyl radical. The differences in energy of the transition states leading to the abstraction of either of the two α- or *β*-hydrogen atoms and resulting from the attack of either side of the benzyl radical are small. The largest energetic differences of up to 0.19 kcal/mol occurred for the hydrogen abstraction by the *p*-methoxy-benzyl radical (reaction 2) on *p*-methoxy-PPE for the reaction paths where the two aromatic rings are closest and steric effects are largest. Even though the energetic differences are small we include these configurations in our investigation since the influence on the Arrhenius prefactors and rate constants might be larger.

The transition states for the hydrogen abstraction on *p*-hydroxy-PPE by the phenoxyl radical are given in Figure 3; the transition states for the hydrogen abstraction by the *p*-hydroxy-benzyl radical are shown in Figure 4. Figure 5 depicts the transition states for the hydrogen abstraction on *p*-methoxy-PPE by the phenoxyl radical and Figure 6 by the *p*-methoxy-benzyl radical. The conformers are equivalent to the ones obtained for the pyrolysis of PPE[3] independent of the substituent. We notice that **TS2**, in which the two aromatic rings that carry the substituents are in close proximity, and **TS3** are interchanged for the equivalent reaction of methoxy-PPE, which has the larger substituent. The transition states for each reaction are distinct by the position of the radical relative to the ether, approximately corresponding to a rotation around the axis of hydrogen transfer. This suggests that multiple transition states could be combined by applying the hindered rotor approximation but the large number of coupled low frequency modes makes it difficult to decouple the internal rotation from the low frequencies and a reaction path is assigned to each transition state.

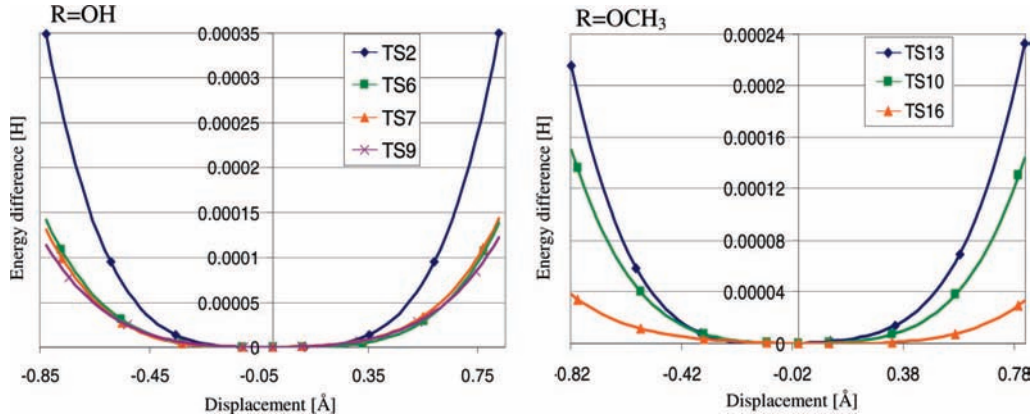

Figure 7. Potentials obtained by displacement along spurious imaginary modes in transition states for the pyrolysis of R-PPE, R = OH,OCH_3.

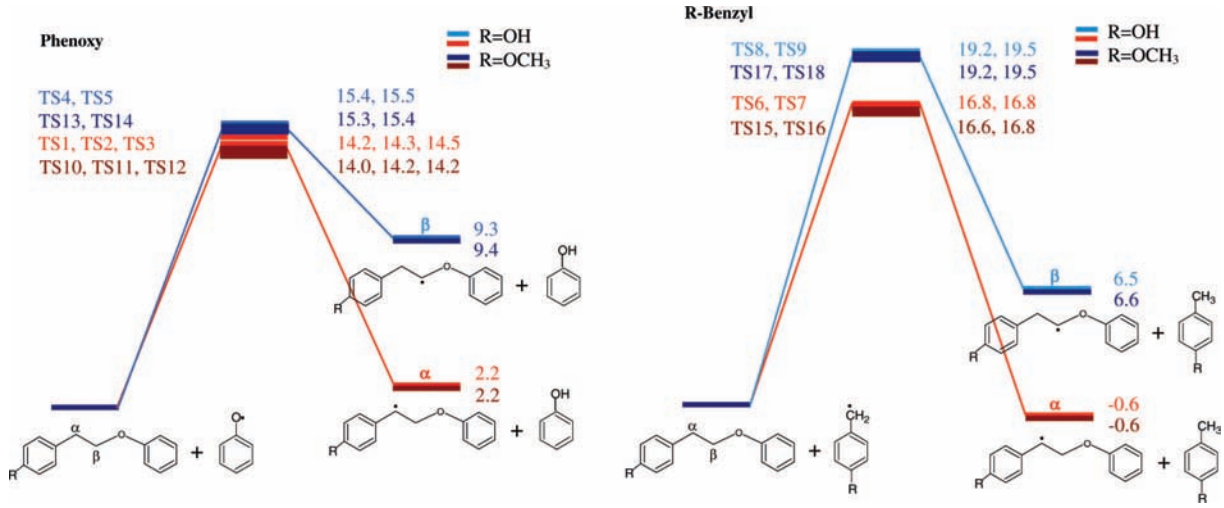

Figure 8. Reaction profile for the hydrogen abstraction on R-PPE by phenoxyl radical (reaction 1) and R-benzyl radical (reaction 2) [R = OH,OCH_3]; energy differences in kcal/mol.

Vibrational analysis showed an average imaginary frequency corresponding to the dissociation of the transition state of *i*1735 cm^{-1} for the transition states of the hydrogen abstraction by the phenoxyl radical and of *i*1682 cm^{-1} for the transition states of the hydrogen abstraction by the R-benzyl radical (R = OH,OCH_3). In addition, we found spurious imaginary frequencies in **TS2**, **TS6**, **TS7**, **TS9**, **TS10**, **TS13**, and **TS16**. These spurious frequencies are small and do not exceed *i*10 cm^{-1}. They are caused by numerical inaccuracies occurring as a consequence of a flat potential energy surface and the break down of the harmonic approximation.[3,14] Figure 7 shows the potentials obtained by displacement along the spurious imaginary modes. For all transition states, the minimum occurs at zero displacement demonstrating that the transition states are saddle points on the potential energy surface.

With the introduction of an oxygen substituent the hydrogen−radical and hydrogen−ether distances (Figures 3 and 6) in the transition states do not vary significantly; within ±0.01 Å compared to PPE.[3] The α-transition states of the R-benzyl abstraction are symmetric with respect to the position of the transferred hydrogen atom, whereas the H-ether distance is larger in the β-transition states. Correspondingly, the energies of the α- and β-transition states for the abstraction by the phenoxyl radical are similar, but the energy barriers for the α- and β-pathways of the abstraction by the R-benzyl radical differ.

Figure 8 shows the reaction profiles for the hydrogen abstraction reactions 1a, 1b, 2a, and 2b for the hydroxy and methoxy substituents. Reaction energies and barriers are similar to the ones calculated for the hydrogen abstraction reactions on PPE.[3] The barrier and reaction energy differences between the hydroxy and methoxy species are very small. The α-radicals are stabilized relative to the β-radicals by delocalization of the unpaired electron, which is enhanced by the hydroxy and methoxy substituents. For R = OH, the energy difference between the α- and β-radicals is 7.1 kcal/mol, which is very similar for R = OCH_3 with 7.2 kcal/mol. The energy difference for unsubstituted PPE is with 6.7 kcal/mol smaller.[3] In the transition states the delocalization is less effective, and most of the spin density is found in the hydrogen bridge. This is not affected by the substituent and has been visualized for PPE by plotting the spin densities of the radicals and transition states.[3] Opposing the delocalization is the polar effect,[21] which occurs in the phenoxyl transition states.[3] We calculate the charge differences between the transition states and the reactants for the lowest transition state of each reaction. In the R-benzyl transition states the total polarization does not significantly change. The electrophilic phenoxyl radical, on the other hand, polarizes the transition states by drawing charge into the phenoxyl ring. The phenoxyl β-transition states are stabilized relative to α-transition states by charge donation from the adjacent ether oxygen which counterbalances the delocalization effect causing the energy barriers for the α- and β-pathways to be similar. Figure 9 gives the charge differences for the lowest phenoxyl transition states for the hydroxy and methoxy substituents. Comparing the charge differences in Figure 9 with the charge differences for the phenoxyl transition states of PPE,[3]

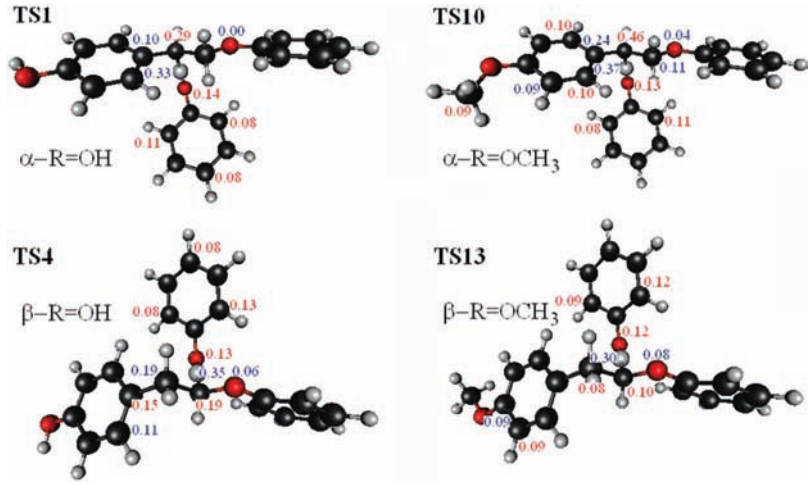

Figure 9. Charge differences [in electrons] between the transition states and the reactants for the lowest transition states of the α- and *β*-pathways of the hydrogen abstraction on R-PPE (R = OH,OCH_3) by phenoxyl (reaction 1). Red, charge gain; blue, charge loss. The display cutoff is 0.08 e^-, except for the ether oxygen, which is always monitored.

TABLE 1: Charge Differences for the Oxygen Atom in the Ether Substituent [in Electrons] between the Transition States and the Reactants for the Lowest Transition States of the α- and *β*-Pathways of the Hydrogen Abstraction on R-PPE by Phenoxyl (reaction 1) and R-Benzyl (reaction 2) for R = OH, OCH_3; Lightface, Charge Gain; Boldface, Charge Loss

	phenoxyl transition states		R-benzyl transition states	
	R = OH	R = OCH_3	R = OH	R = OCH_3
α-pathway	**0.02**	**0.02**	**0.01**	**0.01**
β-pathway	0.01	0.02	**0.01**	0.01

we find that the transition states in Figure 9 are less polarized and that the difference between the charge donation of the ether oxygen in the α- and *β*-transition states (Δq_{ether}) is smaller; R = H, Δq_{ether} = 0.09 e^-; R = OH, Δq_{ether} =0.06 e^-; R = OCH_3, Δq_{ether} = 0.04 e^-. This suggests that the polar effect decreases PPE > PPE-OH ≥ PPE-OCH_3, which corresponds to a small effect in the activation barriers. The energy difference between the lowest α- and *β*-pathways ($\Delta E_{\alpha\beta}$) increases; R = H, $\Delta E_{\alpha\beta}$ = 0.3 kcal/mol; R = OH, $\Delta E_{\alpha\beta}$ = 1.2 kcal/mol; R = OCH_3, $\Delta E_{\alpha\beta}$ = 1.3 kcal/mol.

Additionally, we monitored the charge differences of the hydroxy and methoxy oxygen of the substituent which are given in Table 1. It was suggested in ref 15 that the α-transition states are stabilized by para substituents based on empirical scales. We find the charge effect to be very small, and our results do not indicate that this is an important contribution to the substituent effect in the current case. However, there seems to be a trend that the oxygen atom of the substituent donates charge in the α-transition states and loses charge in the *β*-transition states, which is more pronounced in the more polarized phenoxyl transition states.

B. Kinetic Analysis. Each of the transition states possesses 9−11 frequencies lower than or about 100 cm^{-1} for which we compute the anharmonic potentials along with few anharmonic potentials for low frequencies in the reactants. These potentials are used to calculate the semiclassical vibrational partition functions, for higher frequencies the quantum harmonic approximation is used. Rate constants are calculated using transition-state theory. Figure 10 shows the Arrhenius plots of the rate constants for the hydrogen abstraction reactions on *p*-hydroxy-PPE and *p*-methoxy-PPE. Table 2 gives the Arrhenius prefactors and activation energies obtained from these plots. We recalculated the rate constants for the hydrogen abstraction on PPE[3] for the temperature range of 580−660 K and the data is included in Figure 10 and Table 2. For the hydrogen abstraction by the electrophilic phenoxyl radical we observe a stronger influence of the substituent on the α-pathway than on the *β*-pathway. The abstraction on the α-carbon is accelerated by the substituent and is fastest for methoxy. The abstraction on the *β*-carbon, however, becomes slower. The introduction of the oxygen substituents results in an increase of the α/*β* selectivity for the phenoxyl abstraction which involves a polarized transition state. On the other hand, for the benzyl abstraction, which proceeds through a less-polarized transition state, the substituents decrease the reaction rates for the α- and the *β*-pathways. The α/*β* selectivity is therefore less altered. For the methoxy substituent the *β*-rate is further reduced than the α-rate causing a larger value in the α/*β* selectivity. Table 3 records the α/*β* selectivities for the hydrogen abstraction reactions by the phenoxyl and the R-benzyl radicals on R-PPE (R = H, OH, OCH_3) together with total calculated and experimental α/*β* selectivities, which were measured in a nonpolar biphenyl solvent.[15] The total α/*β* selectivities are computed as described in ref 3, invoking the quasi-steady-state approximation for the free radical chain mechanism. The computed total α/*β* selectivities slightly underestimate the experimental values, but the trend showing the influence of the substituents is reproduced very well.

Finally, we investigated the influence of the different conformers resulting from the inequivalent hydrogen atoms on the α- or *β*-site and from the two inequivalent sides of the substituted benzyl radical (in contrast to their unsubstituted counterparts, see discussion above). We recalculated the rate constants and the α/*β* selectivity for the hydrogen abstraction by the *p*-methoxy-benzyl radical on *p*-methoxy-PPE including pathways through four different conformers of **TS15**, **TS16**, **TS17** and four different conformers of **TS18** yielding an α/*β* selectivity of 8.4. The total α/*β* selectivity stays unchanged with 5.5. This indicates that assuming the two α hydrogen atoms and the two *β* hydrogen atoms, respectively, of *p*-methoxy-PPE are indistinguishable and assuming the two sides of the *p*-methoxy-benzyl radical identical is a good approximation.

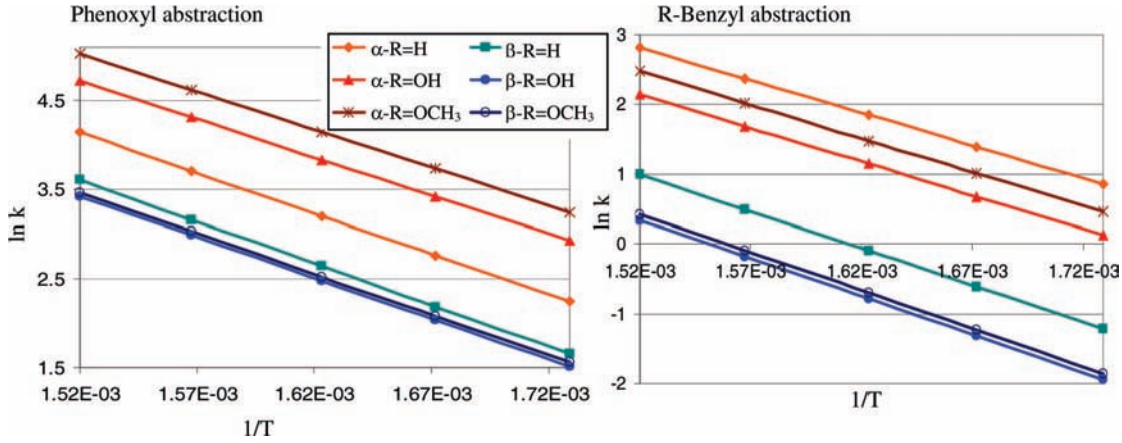

Figure 10. Arrhenius plots for the computed rate constants of the α- and β-pathways of the hydrogen abstraction on R-PPE by the phenoxyl radical (reaction 1) and the R-benzyl radical (reaction 2); R = H, OH, OCH_3.

TABLE 2: Prefactors and Activation Energies Obtained from Arrhenius Plots for the Hydrogen Abstraction on R-PPE (R = H, OH, OCH_3); Temperature Range 580−660 K

		R = H		R = OH		R = OCH_3	
		ln(*A*)	E_a [kcal/mol]	ln(*A*)	E_a [kcal/mol]	ln(*A*)	E_a [kcal/mol]
phenoxyl (reaction 1)	α	17.9	18.0	17.7	17.1	18.0	17.0
	β	17.8	18.6	17.3	18.2	17.3	18.1
R-benzyl (reaction 2)	α	17.1	18.7	16.8	19.2	17.1	19.2
	β	17.1	21.1	16.9	21.7	17.0	21.8

TABLE 3: α/β Selectivities for the Hydrogen Abstraction Reactions by the Phenoxyl and the R-Benzyl Radicals on R-PPE (R = H, OH, OCH_3) at 618 K; Experimental Values from Ref 15

	R = H this work	exptl	R = OH this work	exptl	R = OCH_3 this work	exptl
phenoxyl	1.8		3.9		5.1	
R-benzyl	7.0		6.9		8.9	
total	2.4	3.8 ± 0.3	4.3	5.1 ± 0.1	5.5	7.4 ± 0.3

Conclusion

The transition states for the hydrogen abstraction reactions by the phenoxyl and the R-benzyl radicals on R-PPE (R = OH, OCH_3) have been calculated. The geometries are very similar to the transition-state geometries for the hydrogen abstraction reactions on PPE.[3] We have shown that the α-pathways are stabilized by delocalization of the unpaired electron in the transition states.[3] An opposing trend was found for the abstraction by the polarizing phenoxyl radical (polar effect). The β-transition states are stabilized by charge donation from the adjacent ether oxygen. The charge differences calculated for the transition states of oxygen substituted PPE indicate that the polar effect is less pronounced for *p*-hydroxy-PPE and *p*-methoxy-PPE, which is consistent with a slight reduction of the rates of the β-phenoxyl-pathways.

We calculate the total α/β selectivities for the pyrolysis of oxygen substituted model compounds for the β-O-4 ether linkage in lignin. We use a computational scheme to calculate relative rate constants proposed in ref 3. Rate constants are calculated with transition-state theory where diagonal anharmonic corrections for low frequencies are incorporated employing a semiclassical approximation for the vibrational partition function. The experimental trend of the α/β selectivities in the pyrolysis of the substituted ethers is well reproduced; PPE < *p*-hydroxy-PPE < *p*-methoxy-PPE. This underlines the importance of the kinetic analysis; the energy barriers alone cannot explain the observed trend in the α/β selectivities. The computed total α/β selectivities systematically underestimate the experimental values but are in quite good agreement considering the approximations involved; that is, quasi-steady-state kinetic analysis, potential solvent effects in the pyrolysis studies, and the assumption that hydrogen abstraction by phenethyl radical and interconversion of α- and β-radicals is insignificant.

The detailed kinetic analysis provides new insights into the origin of the substituent effects. The largest effect of the substituents was recorded for the α-pathways of the phenoxyl abstraction. The hydroxy substituent accelerates the rate compared to PPE, which is even more pronounced for the methoxy substituent. For the less electrophilic R-benzyl radicals, the rates of the α-pathways decrease. The rates of the β-pathways of the hydrogen abstraction reactions by either the phenoxyl or the R-benzyl radical on R-PPE (R = OH, OCH_3) decelerate compared to the hydrogen abstraction on PPE.

Acknowledgment. This research was supported by the Division of Chemical Sciences, Geosciences, and Biosciences, Office of Basic Energy Sciences, U.S. Department of Energy, under Contract No. DE-AC05-00OR22725 with Oak Ridge National Laboratory, managed and operated by UT-Battelle, LLC, and in part by ORNL Laboratory Directed Research and Development Funds.

References and Notes

(1) Suhas Carrott, P. J. M.; Ribeiro Carrott, M. M. L. *Bioresour. Technol.* **2007**, *98*, 2301.

(2) Baumling, S.; Broust, F.; Bazer-Bachi, F.; Bourdeaux, T.; Herbinet, O.; Ndiaye, F. T.; Ferrer, M.; Lédé, J. *Int. J. Hydrogen Energy* **2006**, *31*, 2179.

(3) Beste, A.; Buchanan, A. C., III; Britt, P. F.; Hathorn, B. C.; Harrison, R. J. *J. Chem. Phys. A* **2007**, *111*, 12118.

(4) Kawamoto, H; Horigoshi, S.; Saka, S *J. Wood Sci* **2007**, *53*, 168. (a) Kawamoto, H; Horigoshi, S; Saka, S *J. Wood Sci* **2007**, *53*, 268.

(5) Britt, P. F.; Buchanan, A. C., III; Malcolm, E. A. *J. Org. Chem.* **1995**, *60*, 6523.

(6) Simon, P. J.; Eriksson, K.-E.L. *J. Mol. Struct.* **1996**, *384*, 1.

(7) Agache, C.; Popa, V. I. *Mon. Chem.* **2006**, *137*, 55.

(8) Hemelsoet, K.; Speybroeck, V. V.; Moran, D.; Marin, G. B.; Radom, L.; Waroquier, M. *J. Chem. Phys. A* **2006**, *110*, 13624.

(9) Hemelsoet, K.; Moran, D.; Speybroeck, V. V.; Waroquier, M.; Radom, L. *J. Chem. Phys. A* **2006**, *110*, 8942.

(10) Allen, W. D.; Bodi, A.; Szalay, V.; Császár, A. G. *J. Chem. Phys.* **2006**, *124*, 224310.

(11) Willetts, A.; Handy, N. C.; Green, W. H, Jr.; Jayatilaka, D *J. Phys. Chem.* **1990**, *94*, 5608.

(12) Gregurick, S. K.; Chaban, G. M.; Gerber, R. B. *J. Phys. Chem. A* **2002**, *106*, 8696.

(13) Barone, V. *J. Chem. Phys.* **2004**, *120*, 3059.

(14) Beste, A; Buchanan, A. C., III; Britt, P. F.; Hathorn, B. C.; Harrison, R. J *THEOCHEM* **2008**, *851*, 232.

(15) Britt, P. F.; Kidder, M. K.; Buchanan, A. C., III *Energy Fuels* **2007**, *21*, 3102.

(16) Apra, E.et al. *NWChem, A Computational Chemistry Package for Parallel Computers, Version 4.7*; Pacific Northwest National Laboratory; Richland, WA, 2005; pp 99352−0999.

(17) Becke, A. D. *J. Chem. Phys.* **1993**, *98*, 5648.

(18) Lee, C.; Yang, W.; Parr, R. G. *Phys. Rev. B* **1988**, *37*, 785.

(19) McQuarrie, D. A. *Statistical Mechanics; University Science Books*: Sausalito, CA, 2000.

(20) Wigner, E. P *Phys. Rev.* **1932**, *40*, 749. (a) Kirkwood, J. G *Phys. Rev.* **1933**, *44*, 31.

(21) *Free Radicals*; Kochi, J. K., Ed.; John Wiley & Sons, Inc.: New York, NY, 1973; Vol. I.

JP800767J